The FEBS Journal

FEBS PRESS science publishing by scientists

REVIEW ARTICLE

Quantitative imaging and dynamics of tumor therapy with viruses

Iris Kemler[1], Bhargav Karamched[2], Claudia Neuhauser[3] and David Dingli[1,4]

1 Department of Molecular Medicine, Mayo Clinic, Rochester, MN, USA
2 Department of Mathematics and Institute of Molecular Biophysics, Florida State University, Tallahassee, FL, USA
3 Department of Mathematics, University of Houston, TX, USA
4 Division of Hematology and Department of Internal Medicine, Mayo Clinic, Rochester, MN, USA

Keywords
dynamics; fluorescence imaging; molecular imaging; oncolytic virotherapy; replicating viruses

Correspondence
D. Dingli, Mayo Clinic, 200 First Street SW, Rochester, MN 55905, USA
Tel: +507 284 3178
E-mail: dingli.david@mayo.edu

(Received 8 February 2021, revised 7 June 2021, accepted 1 July 2021)

doi:10.1111/febs.16102

Cancer therapy remains challenging due to the myriad presentations of the disease and the vast genetic diversity of tumors that continuously evolve and often become resistant to therapy. Viruses can be engineered to specifically infect, replicate, and kill tumor cells (tumor virotherapy). Moreover, the viruses can be "armed" with therapeutic genes to enhance their oncolytic effect. Using viruses to treat cancer is exciting and novel and in principle can be used for a broad variety of tumors. However, the approach is distinctly different from other cancer therapies since success depends on establishment of an infection within the tumor and ongoing propagation of the oncolytic virus within the tumor itself. Therefore, the target itself amplifies the therapy. This introduces complex dynamics especially when the immune system is taken into consideration as well as the physical and other biological barriers to virus growth. Understanding these dynamics not only requires mathematical and computational models but also approaches for the noninvasive monitoring of the virus and tumor populations. In this perspective, we discuss strategies and current results to achieve this important goal of understanding these dynamics in pursuit of optimization of oncolytic virotherapy.

Introduction

Over the last decades, we have witnessed great progress in the understanding and therapy of cancer ever since the "war on cancer" was declared in 1971 with the signing of the National Cancer Institute Act. A revolution has occurred with the development of many approaches, including preventive therapies, cancer surveillance, organ sparing surgery, and the development of novel therapies, including monoclonal antibodies, targeted therapies such as tyrosine kinase inhibitors, safer chemotherapeutic agents, proton beam therapy, stem cell transplantation and more recently bispecific T-cell engagers, and chimeric antigen receptor-targeted T cells (CAR-T) [1]. These therapeutic modalities have all improved survival for patients with many different tumor types. The field accelerated further with the "omics" revolution, and now the prospect of personalized targeted therapy based on the identification of tumor-specific driver mutations appears to be at hand, at least for some tumors. However, it is also clear that most tumors recur due to the

Abbreviations
CAR-T, chimeric antigen receptor-targeted T cells; CEA, carcinoembryonic antigen; DSFC, dorsal skinfold chamber; EGFR, epidermal growth factor receptor; MV, measles virus; MV-NIS, recombinant measles virus expressing the sodium iodide symporter; PET/CT, positron emission tomography combined with computerized tomography; qRT-PCR, quantitative reverse transcriptase polymerase chain reaction; SPECT, single-photon emission computerized tomography; TCID50, 50% tissue culture infective dose; TFB, tetrafluoroborate.

emergence of resistant subclones that in the presence of therapy are positively selected, leading to disease relapse and ultimately death [2,3]. Therefore, the need for novel therapeutic approaches remains.

An emerging field of tumor therapy is the use of replication competent viruses to treat cancer [4–6]. To date, at least two virus-based therapies have been approved for cancer therapy: Ad-p53 (Gendicine) for head and neck cancer and talimogene laherparepvec (IMLYGIC) for injection in nonresectable malignant melanoma skin lesions and local lymph nodes. Viruses have evolved over millions of years to specifically infect, replicate, and propagate in cells where they hijack the cellular machinery for their own reproduction [4,5,7]. Perhaps fortuitously, many of the mutations that lead to the cancer phenotype are taken advantage of by viruses to enable them to preferentially infect, replicate in, and kill cancer cells [5–7]. Moreover, other viruses can be engineered to exploit differences between normal and cancer cells to spread only within the tumor cell population [8]. These observations have led to the development of tumor virotherapy, where either naturally occurring or engineered viruses are injected in patients with the specific purpose of selectively infecting and replicating within the tumor cell population leading to its demise [5]. Viruses can be engineered to enhance their potency, shielded from the immune response, or to optimally work with combination therapy including immunomodulation [4,9]. Recently, proof of principle that patients with a disseminated malignancy can be cured by a single dose of a replication competent virus was reported [10]. A patient with relapsed and refractory multiple myeloma who had failed essentially every therapeutic modality available, including stem cell transplant, was injected with a single, systemic dose of a recombinant, replication competent measles virus (MV) engineered to express the human thyroidal sodium iodide symporter (MV-NIS), at a dose of 1 x 10^{11} $TCID_{50}$ [10,11]. This single dose of MV-NIS led to disease control (documented by a bone marrow biopsy that did not show any clonal plasma cells, negative positron emission tomography combined with computerized tomography (PET/CT), and normalization of the monoclonal protein studies) without the need for additional therapy for over 5 years [10]. Moreover, recombinant MV has shown promise against a wide variety of other tumor types including non-Hodgkin lymphoma [12], ovarian carcinoma [13], cerebral glioma [14], pancreatic carcinoma [15], pleural mesothelioma [16], medulloblastoma [17], and prostate carcinoma [18] in animal models. The Edmonston vaccine strain of MV enters cells by preferentially binding the viral hemagglutinin (H) protein to CD46 that is overexpressed by many tumor cells [19]. Moreover, the "H" protein can be mutated to negate CD46 binding [20] and re-engineered to specifically bind to target proteins such as CD38 [21,22], CD20 [23], carcinoembryonic antigen (CEA) [24], and epidermal growth factor receptor (EGFR) [25] and therefore restricting entry of the virus to myeloma cells, B cells, colonic tumor cells, and head and neck cancer, respectively. Many other viruses are currently being studied as oncolytic agents including adenovirus [26], herpes simplex virus [27], reovirus virus [28], vesicular stomatitis virus [29], and Coxsackievirus [30] vaccinia virus [31-34] and retroviral vectors [35] among others. A partial list of current clinical trials of oncolytic virotherapy can be found in [36,37]. Moreover, a search in ClinicalTrials.gov using the terms 'cancer' and virotherapy yields a list of 55 clinical trials that are either actively recruiting patients or have recently closed to accrual. Valuable information can be gained from such clinical studies if the site and extent of viral infection and replication could be determined quantitatively.

In order to enable in vivo imaging of an oncolytic virus, we had generated MV-NIS, a replication competent virus that has been engineered to express the human thyroidal sodium iodide symporter (NIS) [11]. NIS expression by infected tumor cells enables them to concentrate radioactive isotopes that serve two purposes: (a) It allows the determination of the *in vivo* biodistribution of the virus-infected cells using single-photon emission computerized tomography (SPECT)/CT with ^{123}I or $^{99m}TcO_4$ or PET/CT imaging when combined with ^{124}I or ^{18}F tetrafluoroborate (TFB) [11,38–41]. Similar observations have been made with adenovirus expressing NIS in other animal models [42,43] and in human studies [44,45]. (b) In addition, administration of ^{131}I enables the killing of tumor cells that are resistant to virus-mediated oncolysis, together with death of neighboring uninfected tumor cells due to a bystander effect [11,38]. The latter is due to the macroscopic path length of the beta particles (electrons) that are emitted during the decay of ^{131}I and that are able to travel across several cell diameters before being absorbed by surrounding tumor cells leading to their death [39]. In principle, other isotopes with more favorable physical characteristics (e.g., physical half-life of the isotope compared to its retention within the tumor, longer path length of the emitted electron or isotopes that decay by alpha particle emission such as astatine [46]) can be used for better disease control [39,42,47,48] providing a multipronged approach to cancer therapy.

The success of therapy in one patient with relapsed multirefractory multiple myeloma mentioned earlier [10] testifies to the promise of the approach of tumor virotherapy but major hurdles remain. Indeed, subsequent patients with advanced multiple myeloma who were treated on the same protocol ($N = 11$) did not achieve such a sustained response [49]. Although many of these patients experienced a reduction in tumor burden, as measured by the size of the monoclonal protein, and had evidence of infection of diverse tumor sites by the virus documented with radionuclide isotope imaging, the responses were transient and they ultimately all progressed over the course of 2 months after MV-NIS administration. Several mechanisms can explain these outcomes, including that (a) the virus could not spread rapidly enough within the tumor sites to achieve long-lasting control of the disease (kinetic limitation), (b) local barriers limited virus spread (physical barriers), (c) eventual immune clearance of the virus led to failure of therapy, and (d) some tumor sites were never infected in the first place allowing the tumor to regrow once the immune system had cleared the virus. It is important to note that the patients studied in this Phase 1 trial did not have pre-existing neutralizing antibodies against MV prior to virus administration. Moreover, imaging studies in these patients confirmed successful infection of macroscopic tumor deposits. However, despite their prior heavy therapies, all patients mounted a robust and specific anti-MV immune response. This implies that oncolytic virotherapy with a specific virus may be a one-shot approach to therapy and patients have to be chosen carefully for optimal results since currently it appears unlikely that a second injection with MV-NIS (or other oncolytic viruses of the same clade) would be possible, unless the virus is pseudotyped to bypass the immune response [50].

If we want to reliably and consistently achieve successful outcomes with these novel therapies, the complex dynamic interactions that exist among the tumor, the virus, and likely immune response as well as the mechanisms and biochemical or biophysical barriers that may hinder or facilitate virus spread and tumor killing need to be understood. In essence, this is the equivalent of classical drug pharmacokinetics but with a twist. Tumor therapy with replicating oncolytic viruses is an exercise in population dynamics [51–66] since the approach in part depends on the amplification of the therapeutic agent (virus) by the target (tumor), a concept that is virtually unique to this approach to therapy (the other exception is immune effector cell therapy, e.g., CAR-T). Both *in vitro* and *in vivo* studies have shown that the outcomes of tumor therapy are highly variable, even when the same cell line is infected *in vitro* and *in vivo* with the same virus [67].

Virotherapy has many moving parts, and a large number of potential therapeutic scenarios exist that make it impossible to perform every plausible experiment in animal models to understand the outcomes. *In silico* studies of such dynamics can be extremely useful to narrow down the universe of possibilities, which reduce the number of *in vivo* studies that need to be performed to test such hypotheses. Therefore, the development of accurate computational models that capture in a realistic fashion the dynamics of such systems is highly desirable. Many models that describe the dynamics of tumor virotherapy exist. Some are based on the Lotka–Volterra "predator–prey" model [53–58,65], and others are based on partial differential equations [59,61,62] that capture diffusion of the virus, while others take into consideration the effect of space [51,68–71] and even include stochastic dynamics [66,68,69,71]. Often these models contain many free parameters, and the data available for fitting are limited and generally restricted to macroscopic values of estimated tumor population size and perhaps some of the "initial conditions." Therefore, the process of data fitting and parameter estimation can be quite challenging, and this ultimately limits the use of such models to make meaningful predictions that can be tested experimentally and incorporated in the process to optimize therapy [64].

Molecular imaging technology that can serially and noninvasively monitor in real time the dynamics of the tumor and virus populations without disturbing the system in the process is a novel approach that can add much-needed spatiotemporal data to greatly improve fitting parameters of the models and thus limit the parameter space for such mathematical modeling. Ideally, these systems can be used in both small animal models as well as large mammals including humans for ease of translation and reproducibility. Several attempts utilized radionuclide-based imaging such as ^{18}F-labeled substrates for thymidine kinase [72], a dopamine D2 receptor [73], the human somatostatin receptor 2 (hSSRT2) [74], the human noreponeprhine transporter (hNET) [75] or the thyroidal sodium iodide symporter (NIS) using both ^{99m}Tc or ^{123}I (SPECT) [39,45] or ^{124}I (PET) [40,43]. Bioluminescence imaging using luciferase as a reporter has also been utilized [76], although translation of this approach into larger animals is difficult. NIS can concentrate a variety of anions (^{123}I, $^{99m}TcO_4$) [39,45] that undergo various types of radionuclide decay leading to the release of gamma photons (SPECT imaging), alpha or beta

particles (^{211}As, ^{131}I, therapeutic) [46], or positrons (^{124}I, ^{18}F TFB) that enable PET imaging [40,43].

Quantitative imaging in tumor virotherapy has been studied using two complementary imaging technologies: SPECT- or PET-based nuclear imaging [15,43,77–82] and, more recently, fluorescence-based imaging at a single-cell resolution using the implantable dorsal skinfold chamber (DSFC) with fluorescently labeled cells [83]. We discuss both in the following in detail.

Nuclear imaging

The initial attempts at *in vivo* tracking of oncolytic virus spread depended on NIS expression by virus-infected tumor cells that concentrate radioactive isotopes for serial *in vivo* imaging [84]. This approach may be suitable for human studies since the technology is already approved for use in humans and we have evidence of the applicability of this approach in clinical trials [10,49]. The fundamental concept is that infection of cancer cells by the oncolytic virus induces NIS expression that will lead to radioisotope uptake by the cells. Imaging using SPECT (or PET) will be able to quantify the isotope concentration in the tumor, and this will in turn be *related* to the amount of virus present in the tumor at that time [43,81,82]. Serial imaging should then provide information on the dynamics of the virus-infected cell population and indirectly about the oncolytic virus itself. Critical to this approach are the following features: (a) low to absent background isotope uptake/activity in the tumor, (b) rapid isotope elimination due to decay so as to prevent spillover effect from serial imaging [39], (c) the isotope has no impact on the virus population, and (d) reproducible and accurate quantification of the isotope activity in the tumor based on imaging [77,78].

Pictorially, the hypothesis is shown in Fig. 1A with a series of steps that follow logically one after the other. Initially, the hypothesis was tested *in vitro* by infecting tumor cells and assessing them for NIS expression both by radioactive isotope uptake and by gene expression using quantitative reverse transcriptase polymerase chain reaction (qRT-PCR) (Fig. 1B) [77]. Parallel serial studies also were performed to measure viable virus production and release from infected cells by titration of the collected supernatant on Vero cells.

In order to ensure that the results were robust and reproducible, two virus-encoded genes were quantitated—the "N" gene which is a structural viral gene and NIS itself (the reporter gene) (Fig. 1C). The genomic organization of MV-NIS is presented in Fig. 2. It is important to note that with this genome structure, one expects a higher level of "N" gene expression compared with "NIS" due to the "stuttering" of the viral polymerase when it reaches the end of each transcriptional unit present in the viral genome. We observed a strong linear relationship between infectious virus particles, viral N and NIS expression, and radioactive isotope uptake. Therefore, it appears that *in vitro* the hypothesis is correct.

Proving an association between isotope uptake and virus population *in vivo* (Fig. 1D) is experimentally more difficult due to the variability of infection within the tumor, the loss of signal from isotope due to tissue attenuation, and anisotropies between infected foci within the tumor. It is essential to establish that SPECT/CT imaging can accurately quantitate the isotope activity within the tumor. Therefore, once the imaging data were captured, each mouse was euthanized, the tumor was excised, and the activity in the tumor was measured using a dose calibrator (Fig. 3). There was a high degree of correlation between the activity as measured by SPECT/CT imaging and the dose calibrator [77]. This is similar to what had been reported by Carlson *et al.* [78]. Similar observations have been made with PET based imaging using ^{124}I in combination with NIS [43].

In vivo, a high correlation between viral "N" and "NIS" gene expression [77] was observed which suggests that the virus is behaving similarly *in vitro* and *in vivo*. The intratumoral concentration of radioactive isotope also correlated well with the levels of viral gene expression. Parts of the excised tumors were lysed, and virus was isolated. Viable virus was detected in all tumors isolated from mice injected with the oncolytic virus but in none of the controls. Moreover, while the control tumors did not express NIS to any extent (1.5 copies·ng^{-1} RNA), the transgene was expressed in all tumors infected with the virus (76.9 copies·ng^{-1} RNA, $P = 0.001$). As a consequence, isotope uptake mediated by NIS was significantly higher than background isotope activity in the control tumors, as also reported by other groups with other vector systems such as adenovirus [44,45,84], vesicular stomatitis virus [85] and vaccinia virus [86]. These observations are also supported by independent studies which showed that using a threshold of 1.5 times over the background activity of the isotope in the tumor could reliably predict that 2.7% of the tumor cells are infected with the oncolytic virus [79]. A significant correlation between the virus population isolated from the tumors and isotope uptake was found; however, it was lower than what had been observed *in vitro*. What could account for these differences?

Potential explanations were identified from the *in vivo* experiments, in which two MV-derived

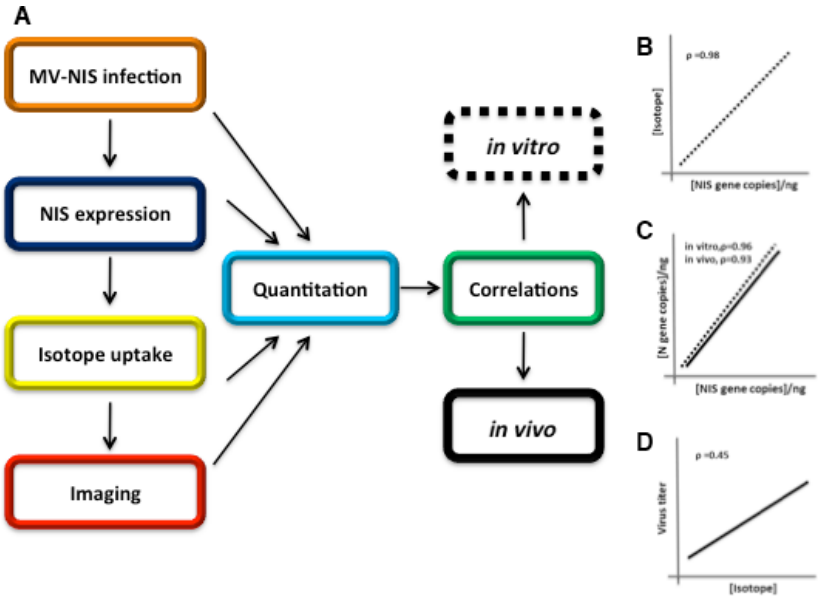

Fig. 1. *In vitro* and *in vivo* correlations between reporter gene function and virus infection of tumor cells. In (A), we present the general hypothesis and experimental schema to determine whether in vivo imaging can be used to predict intratumoral oncolytic virus concentrations. In vivo correlations between (B) NIS mediated isotope uptake in the tumor and NIS gene expression, (C) viral 'N' gene and 'NIS' gene expression within the tumor xenografts and (D) intratumoral viable virus recovery versus isotope concentration. Strong positive correlations are found between all parameters, thus supporting our hypothesis.

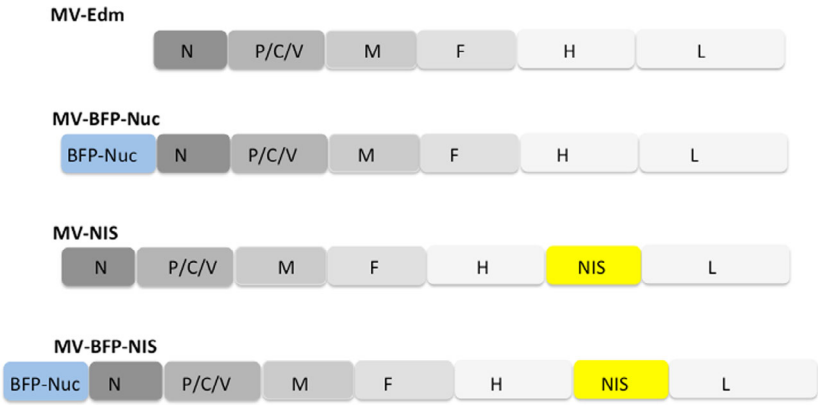

Fig. 2. Schematic representation of the genome organization of the MV and its recombinant derivatives used in our studies. MV-Edm has 6 genes that are transcribed starting from the "N" (highest number of copies) to the "L" which is the viral RNA-dependent RNA polymerase. Additional transcription units can be introduced to add more genes such as blue fluorescent protein (BFP) upstream of "N" or the sodium iodide symporter (NIS), downstream of "H." One of our vectors has both additional genes present to enable both fluorescent-based imaging and nuclide-based imaging of infected tumor cells.

oncolytics were studied: MV-NIS [11] and MV-I98A-NIS. The latter virus is derived from MV-NIS by a mutation in the viral hemagglutinin (H) gene with isoleucine (I) being replaced by alanine (A) at position 98. The phenotypic effect of this mutation is a reduced ability of the virus to fuse cells together [87,88], and consequently, infected cells are killed more slowly. Tumors infected with MV-I98A-NIS had higher *in vivo* isotope activity although the peak was reached at a later time point due to slower kinetics of spread. This suggests that apart from the dynamics of the virus, the rate of expression of the transgene and how long the infected cells remain alive can have an impact on the ability to image and quantify the infected cell burden *in vivo*. Moreover, there is likely a threshold level of NIS expression that is needed for isotope to be concentrated in the tumor and detectable by SPECT/CT imaging [89].

The *in vivo* scenario introduces additional new variables that can influence the correlations between virus population and isotope uptake including (a) differences in the speed of replication and spread within the tumor

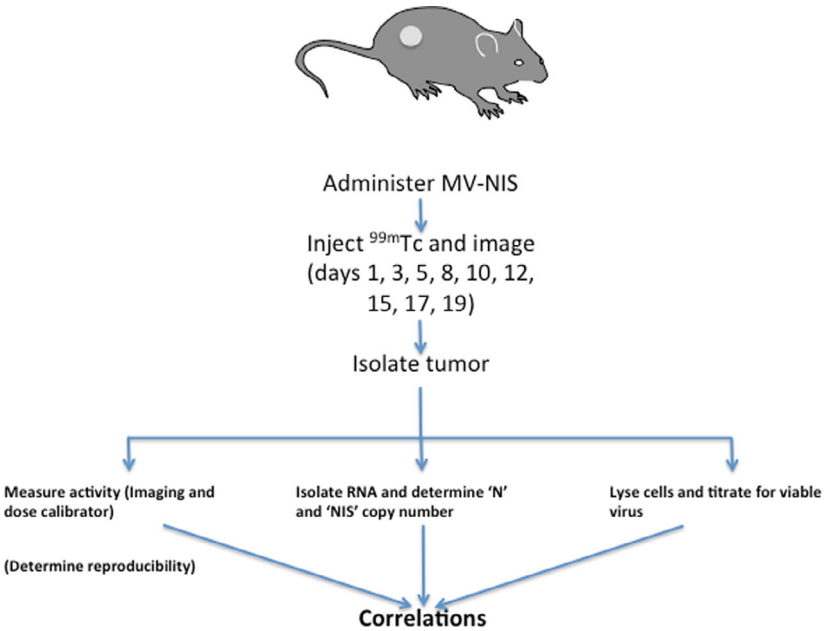

Fig. 3. *In vivo* experimental schema for the described experiments. After establishment of tumor xenografts in nude mice, the tumors are injected with MV-NIS and subsequently injected with ^{99m}Tc for imaging using SPECT/CT. Quantitation of intratumoral isotope is performed both by imaging and by dose counter of the excised tumor. The tumor is subsequently divided into parts to enable isolation of RNA for viral gene quantitation as well as titration for viable virus.

and (b) anisotropies in the distribution of the virus. There is some evidence that the spatial relationships between cells may impact isotope retention by the tumor due to possible recycling of the isotope [90]. If this is true, then the spatial distribution of the infected cells with respect to one another becomes quite important. Unfortunately, the resolution provided by micro-SPECT/CT is not enough to allow proper quantification of the size of the infected tumor foci [79] and imaging techniques with a higher resolution are needed. This is clearly an example where the average is not good enough since significant differences across animals and between metastatic tumor deposits within the same animal can be expected due to spatial anisotropies and stochastic effects with respect to both the tumor cells and the sites of tumor cell infection by the virus [77,79,80,91]. It is likely that accurate *determination* of the number of tumor cells, how many of them are infected, and the spatial distribution of infected cells within the tumor environment is required for better understanding of isotope-based imaging data.

Fluorescence imaging

Fluorescence-based imaging can provide single-cell resolution, and, in principle, quantify the number of cells in a given volume. With the advent of multiphoton microscopy and the use of the DSFC [92], it is possible to determine *in vivo* the number of cells present in a specific volume of tumor. This technology was applied to determine oncolytic virus dynamics *in vivo* using the two MV platforms mentioned: MV-Edm and MV-I98A but engineered to express fluorescent proteins in the nucleus of infected cells [93] (blue in Fig. 4). Nuclear localization facilitates the discrimination between individual cells and enables counting of the number of cells in a focus of infection. Tumor cells that express a different fluorophore without restriction to the nucleus (red in Fig. 4) were used as targets of infection. Experimentally, tumor cells were injected subcutaneously in the flank of athymic mice and once the tumors reached a diameter of ~ 0.4 cm, the DSFC was inserted over the tumor xenograft under anesthesia. The oncolytic virus was subsequently injected in the tumor volume and imaging started 24 h later using a multiphoton microscope with the mouse held in a restrainer under inhalational anesthesia (isoflurane) and with passive warming. The observations obtained using this approach were insightful and also illustrated some of the persistent barriers to successful tumor therapy with viruses.

The oncolytic viruses established multiple foci of infection within the tumor and were able to spread to adjacent cells. Spread could be quite rapid, especially with the fusogenic virus (MV-Edm) (Fig. 4C–F) that can eliminate sheets of tumor cells over the course of a few days. In combination with image analysis software such as Imaris^{TM}, it was possible to determine the number of cells in any focus of infection and how this changed in time (Fig. 4G–J). However, despite the presence of high-level infection, many areas within the tumor may remain uninfected. It is currently not clear whether this relates to the dose of virus injected or to the fact the injection is within the tumor itself. It is well known

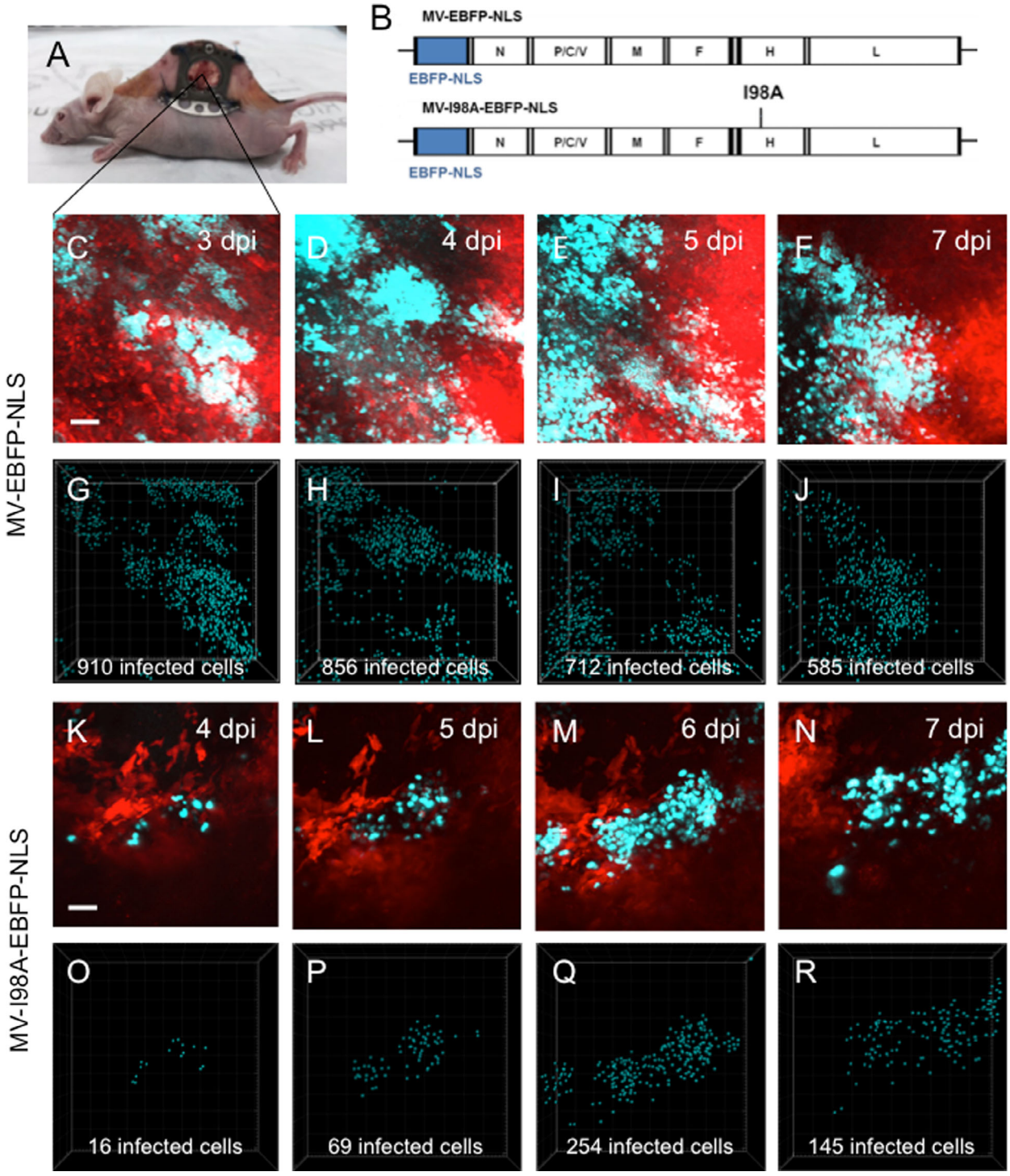

Fig. 4. Fluorescent-based imaging of MV replication *in vivo*. (A) Athymic nude mouse with a DSFC implanted. (B) Schematic representation of the plasmids coding for the measles virus MV-EBFP-NLS (fusogenic) and MV-I98A-EBFP-NLS (hypofusogenic) genomes. (C–F) Maximum-intensity projections of HT1080-tdTomato tumors (red) grown in the DSFC and infected with MV-EBFP-NLS (blue nuclei), imaged at day 3 (C), day 4 (D), day 5 (E), and day 7 (F) postinfection. Scale bars, 50 μm. (G-J) The number of infected cells was determined by counting blue nuclei with the Imaris spot analysis software. (K-N) Maximum-intensity projections of HT1080-tdTomato tumors grown in the DSFC and infected with MV-I98A-EBFP-NLS, imaged at day 4 (K), day 5 (L), day 6 (M), and day 7 (N) postinfection. (O-R) The number of infected cells was determined with the IMARIS SPOT ANALYSIS software.

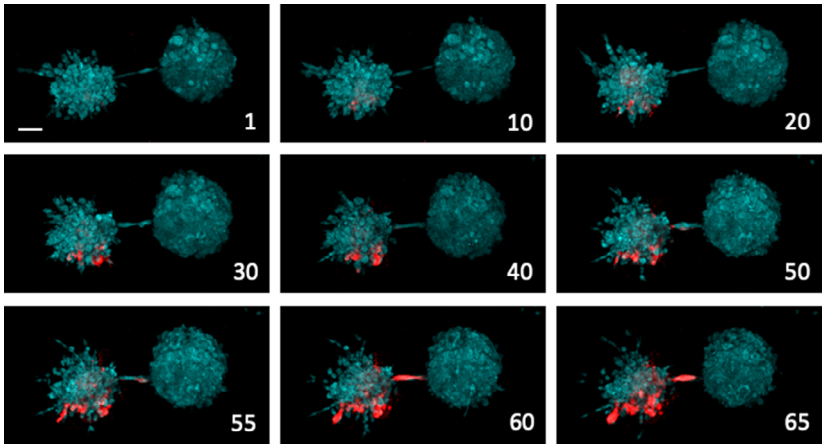

Fig. 5. Spread of infection between tumor spheroids via nanotubes. HT1080 tumor spheroids (expressing CFP) were generated and infected with MV-Red (Cherry/tdTom), MOI 1. Z-stacks were acquired with a confocal microscope at the indicated times (hours) postinfection. Projections from one spheroid to another (blue) are visible that turn red (timeframes 55, 60, and 65) presumably due to spread of the virus. The scale bar represents 100 μm.

that systemic delivery of the virus is possible and can establish infection within tumor xenografts [11,67]. Interestingly, rapid tumor cell death, such as with vesicular stomatitis virus, can lead to the development of voids within the tumor that represent volumes that do not contain any tumor cells [80,94]. Perhaps this leads to the cessation of virus spread since the infection foci lose contact with the rest of the tumor. Systemic delivery may be expected to produce a more uniform infection within the tumor [94] that could improve spread of the virus and its oncolytic effect [79]. One model has suggested that diffusion is a major limitation of viral spread *in vivo* [59] and in such a scenario, having multiple foci of infection at the time of administration is likely to be critical. Spread of infection via cell to cell fusion appears to enable faster propagation of the virus, and over the same timescale, the number of infected cells and the area under curve are higher compared with the slower and less fusogenic-mutant virus MV-I98A [93]. Recently, it was reported that some viruses can spread from cell to cell via nanotubes that allow cell–cell interactions [95–97]. Although we have observed what appears to be the transport of cytoplasmic material in nanotubes in vitro using cultured tumor spheroids (Fig. 5), to date, our studies have not documented this method of spread in vivo.

Combined approaches

While fluorescent-based imaging is able to accurately determine the size of infected foci, the approach cannot be used for orthotopic models or translated into larger mammals. However, combining fluorescent-based imaging with nuclear imaging in small animals may provide an optimal way to answer fundamental questions with respect to tumor virotherapy that can be more easily translated into larger mammals. Specifically, what is the minimum size of an infection focus that can be reliably imaged with SPECT/CT? Can the virus population be inferred from the isotope concentration within the tumor as determined by imaging? What is the best time window to monitor viral spread? How do the dynamics of cell killing impact the ability to image the foci of infection? Is it better to have many cells infected at a low level or a smaller number of cells infected that express NIS at a high level for optimal imaging? Is the latter option superior if a therapeutic radionuclide is added to enhance the cytoreductive effect of the virus on the tumor [11,15]? When would be the optimal time to intervene with a therapeutic radionuclide and what would be the best dose to maximize tumor cell killing? In the era of imaging-based approaches to personalized cancer therapy, answering such questions would be of fundamental importance.

These questions can be addressed with a recombinant MV that expresses both a fluorescent protein in infected cells as well as NIS (Fig. 2) and a DSFC that is made of plastic to minimize interference with imaging. Fluorescent imaging will determine the distribution and number of infected cells. Immediately after, the same mice can be injected with ^{99m}Tc and imaged using micro-CT/SPECT. Isotope uptake in the tumors may be correlated with the number of infected cells in the tumor determined by fluorescent imaging, the distribution of the infected cells in space (Fig. 4), and the lifespan of infected cells.

Cancer therapy with viruses or CAR-T is more complex than the use of chemotherapy or antibodies. Outcomes are determined by the dynamic interactions of the populations, and determining the size of such

populations as a function of time will be critical for optimization of therapy. Combined imaging modalities should provide vitally important insights into these dynamics and planning of future therapies. At the same time, many investigators are developing approaches to surmount immunologic and physical barriers to successful tumor virotherapy. Some potential solutions include the use of cells as carriers of oncolytic viruses [98–100], altering the tumor microenvironment using immune checkpoint inhibitors [101] or immunomodulatory drugs such as cyclophosphamide or ruxolitinib [102,103] and engineering oncolytic viruses to express enzymes which can disrupt the extracellular matrix that can interfere with local virus spread within tumors [104,105].

Acknowledgements

This work was in part supported by R01 CA184241 (NCI) and Grant 09.03 from the Minnesota Partnership for Biotechnology and Medical Genomics.

Conflict of interest

The authors declare no conflict of interest.

Author contributions

All the authors contributed to the concepts, approaches, and discussions in relation to this article and meet all criteria for authorship. The manuscript was written by DD with critical input from all the co-authors.

References

1 June CH & Sadelain M (2018) Chimeric antigen receptor therapy. *The N Engl J Med* **379**, 64–73.
2 Foo J & Michor F (2009) Evolution of resistance to targeted anti-cancer therapies during continuous and pulsed administration strategies. *PLoS Comput Biol* **5**, e1000557.
3 Watson PA, Arora VK & Sawyers CL (2015) Emerging mechanisms of resistance to androgen receptor inhibitors in prostate cancer. *Nat Rev Cancer* **15**, 701–711.
4 Miest TS & Cattaneo R (2014) New viruses for cancer therapy: meeting clinical needs. *Nat Rev Microbiol* **12**, 23–34.
5 Kelly E & Russell SJ (2007) History of oncolytic viruses: genesis to genetic engineering. *Mol Ther* **15**, 651–659.
6 Kirn D, Martuza RL & Zwiebel J (2001) Replication-selective virotherapy for cancer: biological principles, risk management and future directions. *Nat Med* **7**, 781–787.
7 Lichty BD, Power AT, Stojdl DF & Bell JC (2004) Vesicular stomatitis virus: re-inventing the bullet. *Trends Mol Med* **10**, 210–216.
8 Fukuhara H, Ino Y & Todo T (2016) Oncolytic virus therapy: a new era of cancer treatment at dawn. *Cancer Sci* **107**, 1373–1379.
9 Cattaneo R, Miest T, Shashkova EV & Barry MA (2008) Reprogrammed viruses as cancer therapeutics: targeted, armed and shielded. *Nat Rev Microbiol* **6**, 529–540.
10 Russell SJ, Federspiel MJ, Peng KW, Tong C, Dingli D, Morice WG, Lowe V, O'Connor MK, Kyle RA, Leung N *et al.* (2014) Remission of disseminated cancer after systemic oncolytic virotherapy. *Mayo Clin Proc* **89**, 926–933.
11 Dingli D, Peng KW, Harvey ME, Greipp PR, O'Connor MK, Cattaneo R, Morris JC & Russell SJ (2004) Image-guided radiovirotherapy for multiple myeloma using a recombinant measles virus expressing the thyroidal sodium iodide symporter. *Blood* **103**, 1641–1646.
12 Grote D, Russell SJ, Cornu TI, Cattaneo R, Vile R, Poland GA & Fielding AK (2001) Live attenuated measles virus induces regression of human lymphoma xenografts in immunodeficient mice. *Blood* **97**, 3746–3754.
13 Galanis E, Atherton PJ, Maurer MJ, Knutson KL, Dowdy SC, Cliby WA, Haluska P Jr, Long HJ, Oberg A, Aderca I *et al.* (2015) Oncolytic measles virus expressing the sodium iodide symporter to treat drug-resistant ovarian cancer. *Cancer Res* **75**, 22–30.
14 Opyrchal M, Allen C, Iankov I, Aderca I, Schroeder M, Sarkaria J & Galanis E (2012) Effective radiovirotherapy for malignant gliomas by using oncolytic measles virus strains encoding the sodium iodide symporter (MV-NIS). *Hum Gene Ther* **23**, 419–427.
15 Penheiter AR, Wegman TR, Classic KL, Dingli D, Bender CE, Russell SJ & Carlson SK (2010) Sodium iodide symporter (NIS)-mediated radiovirotherapy for pancreatic cancer. *AJR Am J Roentgenol* **195**, 341–349.
16 Li H, Peng KW, Dingli D, Kratzke RA & Russell SJ (2010) Oncolytic measles viruses encoding interferon beta and the thyroidal sodium iodide symporter gene for mesothelioma virotherapy. *Cancer Gene Ther* **17**, 550–558.
17 Hutzen B, Pierson CR, Russell SJ, Galanis E, Raffel C & Studebaker AW (2012) Treatment of medulloblastoma using an oncolytic measles virus encoding the thyroidal sodium iodide symporter shows enhanced efficacy with radioiodine. *BMC Cancer* **12**, 508.
18 Msaouel P, Iankov ID, Allen C, Aderca I, Federspiel MJ, Tindall DJ, Morris JC, Koutsilieris M, Russell SJ

& Galanis E (2009) Noninvasive imaging and radiovirotherapy of prostate cancer using an oncolytic measles virus expressing the sodium iodide symporter. *Mol Ther* **17**, 2041–2048.

19 Ong HT, Timm MM, Greipp PR, Witzig TE, Dispenzieri A, Russell SJ & Peng KW (2006) Oncolytic measles virus targets high CD46 expression on multiple myeloma cells. *Exp Hematol* **34**, 713–720.

20 Vongpunsawad S, Oezgun N, Braun W & Cattaneo R (2004) Selectively receptor-blind measles viruses: Identification of residues necessary for SLAM- or CD46-induced fusion and their localization on a new hemagglutinin structural model. *J Virol* **78**, 302–313.

21 Nakamura T, Peng KW, Harvey M, Greiner S, Lorimer IA, James CD & Russell SJ (2005) Rescue and propagation of fully retargeted oncolytic measles viruses. *Nat Biotechnol* **23**, 209–214.

22 Peng KW, Donovan KA, Schneider U, Cattaneo R, Lust JA & Russell SJ (2003) Oncolytic measles viruses displaying a single-chain antibody against CD38, a myeloma cell marker. *Blood* **101**, 2557–2562.

23 Bucheit AD, Kumar S, Grote DM, Lin Y, von Messling V, Cattaneo RB & Fielding AK (2003) An oncolytic measles virus engineered to enter cells through the CD20 antigen. *Mol Ther* **7**, 62–72.

24 Hammond AL, Plemper RK, Zhang J, Schneider U, Russell SJ & Cattaneo R (2001) Single-chain antibody displayed on a recombinant measles virus confers entry through the tumor-associated carcinoembryonic antigen. *J Virol* **75**, 2087–2096.

25 Zaoui K, Bossow S, Grossardt C, Leber MF, Springfeld C, Plinkert PK, von Kalle C & Ungerechts G (2012) Chemovirotherapy for head and neck squamous cell carcinoma with EGFR-targeted and CD/UPRT-armed oncolytic measles virus. *Cancer Gene Ther* **19**, 181–191.

26 Li W, Tan J, Wang P, Li N & Li C (2015) Glial fibrillary acidic protein promoters direct adenovirus early 1A gene and human telomerase reverse transcriptase promoters direct sodium iodide symporter expression for malignant glioma radioiodine therapy. *Mol Cell Biochem* **399**, 279–289.

27 Grigg C, Blake Z, Gartrell R, Sacher A, Taback B & Saenger Y (2016) Talimogene laherparepvec (T-Vec) for the treatment of melanoma and other cancers. *Semin Oncol* **43**, 638–646.

28 Sborov DW, Nuovo GJ, Stiff A, Mace T, Lesinski GB, Benson DM Jr, Efebera YA, Rosko AE, Pichiorri F, Grever MR *et al.* (2014) A phase I trial of single-agent reolysin in patients with relapsed multiple myeloma. *Clin Cancer Res* **20**, 5946–5955.

29 Naik S, Nace R, Barber GN & Russell SJ (2012) Potent systemic therapy of multiple myeloma utilizing oncolytic vesicular stomatitis virus coding for interferon-beta. *Cancer Gene Ther* **19**, 443–450.

30 Au GG, Lincz LF, Enno A & Shafren DR (2007) Oncolytic Coxsackievirus A21 as a novel therapy for multiple myeloma. *Br J Haematol* **137**, 133–141.

31 Haddad D, Chen CH, Carlin S, Silberhumer G, Chen NG, Zhang Q, Longo V, Carpenter SG, Mittra A, Carson J *et al.* (2012) Imaging characteristics, tissue distribution, and spread of a novel oncolytic vaccinia virus carrying the human sodium iodide symporter. *PLoS One* **7**, e41647.

32 Breitbach CJ, Burke J, Jonker D, Stephenson J, Haas AR, Chow LQ, Nieva J, Hwang TH, Moon A, Patt R *et al.* (2011) Intravenous delivery of a multi-mechanistic cancer-targeted oncolytic poxvirus in humans. *Nature* **477**, 99–102.

33 Evgin L, Acuna SA, Tanese de Souza C, Marguerie M, Lemay CG, Ilkow CS, Findlay CS, Falls T, Parato KA, Hanwell D *et al.* (2015) Complement inhibition prevents oncolytic vaccinia virus neutralization in immune humans and cynomolgus macaques. *Mol Ther* **23**, 1066–1076.

34 Parato KA, Breitbach CJ, Le Boeuf F, Wang J, Storbeck C, Ilkow C, Diallo JS, Falls T, Burns J, Garcia V *et al.* (2012) The oncolytic poxvirus JX-594 selectively replicates in and destroys cancer cells driven by genetic pathways commonly activated in cancers. *Mol Ther* **20**, 749–758.

35 Kubo S, Takagi-Kimura M, Tagawa M & Kasahara N (2019) Dual-vector prodrug activator gene therapy using retroviral replicating vectors. *Cancer Gene Ther* **26**, 128–135.

36 Pol JG, Levesque S, Workenhe ST, Gujar S, Le Boeuf F, Clements DR, Fahrner JE, Fend L, Bell JC, Mossman KL *et al.* (2018) Trial Watch: Oncolytic viro-immunotherapy of hematologic and solid tumors. *Oncoimmunology* **7**, e1503032.

37 Pelin A, Wang J, Bell J & Le Boeuf F (2017) The importance of imaging strategies for pre-clinical and clinical in vivo distribution of oncolytic viruses. *Oncolytic Virother* **7**, 25–35.

38 Dingli D, Diaz RM, Bergert ER, O'Connor MK, Morris JC & Russell SJ (2003) Genetically targeted radiotherapy for multiple myeloma. *Blood* **102**, 489–496.

39 Dingli D, Russell SJ & Morris JC 3rd (2003) In vivo imaging and tumor therapy with the sodium iodide symporter. *J Cell Biochem* **90**, 1079–1086.

40 Dingli D, Kemp BJ, O'Connor MK, Morris JC, Russell SJ & Lowe VJ (2006) Combined I-124 positron emission tomography/computed tomography imaging of NIS gene expression in animal models of stably transfected and intravenously transfected tumor. *Mol Imaging Biol* **8**, 16–23.

41 Zhang L, Suksanpaisan L, Jiang H, DeGrado TR, Russell SJ, Zhao M & Peng KW (2019) Dual-Isotope SPECT Imaging with NIS reporter gene and

duramycin to visualize tumor susceptibility to oncolytic virus infection. *Mol Ther Oncolytics* **15**, 178–185.

42 Willhauck MJ, Sharif Samani BR, Gildehaus FJ, Wolf I, Senekowitsch-Schmidtke R, Stark HJ, Goke B, Morris JC & Spitzweg C (2007) Application of 188rhenium as an alternative radionuclide for treatment of prostate cancer after tumor-specific sodium iodide symporter gene expression. *J Clin Endocrinol Metab* **92**, 4451–4458.

43 Groot-Wassink T, Aboagye EO, Glaser M, Lemoine NR & Vassaux G (2002) Adenovirus biodistribution and noninvasive imaging of gene expression in vivo by positron emission tomography using human sodium/iodide symporter as reporter gene. *Hum Gene Ther* **13**, 1723–1735.

44 Barton KN, Stricker H, Brown SL, Elshaikh M, Aref I, Lu M, Pegg J, Zhang Y, Karvelis KC, Siddiqui F *et al.* (2008) Phase I study of noninvasive imaging of adenovirus-mediated gene expression in the human prostate. *Mol Ther* **16**, 1761–1769.

45 Barton KN, Tyson D, Stricker H, Lew YS, Heisey G, Koul S, de la Zerda A, Yin FF, Yan H, Nagaraja TN *et al.* (2003) GENIS: gene expression of sodium iodide symporter for noninvasive imaging of gene therapy vectors and quantification of gene expression in vivo. *Mol Ther* **8**, 508–518.

46 Willhauck MJ, Samani BR, Wolf I, Senekowitsch-Schmidtke R, Stark HJ, Meyer GJ, Knapp WH, Goke B, Morris JC & Spitzweg C (2008) The potential of 211Astatine for NIS-mediated radionuclide therapy in prostate cancer. *Eur J Nucl Med Mol Imaging* **35**, 1272–1281.

47 Lehner S, Lang C, Kaissis G, Todica A, Zacherl MJ, Boening G, Spitzweg C, Herbach N, Franz WM, Krause BJ, Steinhoff G, Bartenstein P, Hacker M & David R (2015) I-PET assessment of human sodium iodide symporter reporter gene activity for highly sensitive in vivo monitoring of teratoma formation in Mice. *Mol Imaging Biol*.

48 Petrich T, Quintanilla-Martinez L, Korkmaz Z, Samson E, Helmeke HJ, Meyer GJ, Knapp WH & Potter E (2006) Effective cancer therapy with the alpha-particle emitter [211At]astatine in a mouse model of genetically modified sodium/iodide symporter-expressing tumors. *Clin Cancer Res* **12**, 1342–1348.

49 Dispenzieri A, Tong C, LaPlant B, Lacy MQ, Laumann K, Dingli D, Zhou Y, Federspiel MJ, Gertz MA, Hayman S *et al.* (2017) Phase I trial of systemic administration of Edmonston strain of measles virus genetically engineered to express the sodium iodide symporter in patients with recurrent or refractory multiple myeloma. *Leukemia* **31**, 2791–2798.

50 Munoz-Alia MA, Nace RA & Russell SJ (2020) A measles virus vector pseudotyped with CD46-retargeted canine distemper envelope achieves oncolysis in the presence of measles-immune human serum. *Mol Ther* **28**, 588–588.

51 Wodarz D (2013) Computational modeling approaches to studying the dynamics of oncolytic viruses. *Math Biosci Eng* **10**, 939–957.

52 Wodarz D (2009) Use of oncolytic viruses for the eradication of drug-resistant cancer cells. *J R Soc Interface* **6**, 179–186.

53 Wodarz D (2003) Gene therapy for killing p53-negative cancer cells: use of replicating versus nonreplicating agents. *Hum Gene Ther* **14**, 153–159.

54 Dingli D, Offord C, Myers R, Peng KW, Carr TW, Josic K, Russell SJ & Bajzer Z (2009) Dynamics of multiple myeloma tumor therapy with a recombinant measles virus. *Cancer Gene Ther* **16**, 873–882.

55 Dingli D, Cascino MD, Josic K, Russell SJ & Bajzer Z (2006) Mathematical modeling of cancer radiovirotherapy. *Math Biosci* **199**, 55–78.

56 Rommelfanger DM, Offord CP, Dev J, Bajzer Z, Vile RG & Dingli D (2012) Dynamics of melanoma tumor therapy with vesicular stomatitis virus: explaining the variability in outcomes using mathematical modeling. *Gene Ther* **19**, 543–549.

57 Wu JT, Byrne HM, Kirn DH & Wein LM (2001) Modeling and analysis of a virus that replicates selectively in tumor cells. *Bull Math Biol* **63**, 731–768.

58 Wu JT, Kirn DH & Wein LM (2004) Analysis of a three-way race between tumor growth, a replication-competent virus and an immune response. *Bull Math Biol* **66**, 605–625.

59 Mok W, Stylianopoulos T, Boucher Y & Jain RK (2009) Mathematical modeling of herpes simplex virus distribution in solid tumors: implications for cancer gene therapy. *Clin Cancer Res* **15**, 2352–2360.

60 Brown MC, Dobrikova EY, Dobrikov MI, Walton RW, Gemberling SL, Nair SK, Desjardins A, Sampson JH, Friedman HS, Friedman AH *et al.* (2014) Oncolytic polio virotherapy of cancer. *Cancer* **120**, 3277–3286.

61 Friedman A, Tian JP, Fulci G, Chiocca EA & Wang J (2006) Glioma virotherapy: effects of innate immune suppression and increased viral replication capacity. *Cancer Res* **66**, 2314–2319.

62 Crivelli JJ, Foldes J, Kim PS & Wares JR (2012) A mathematical model for cell cycle-specific cancer virotherapy. *J Biol Dyn* **6** (Suppl 1), 104–120.

63 Komarova NL & Wodarz D (2010) ODE models for oncolytic virus dynamics. *J Theor Biol* **263**, 530–543.

64 Biesecker M, Kimn JH, Lu H, Dingli D & Bajzer Z (2010) Optimization of virotherapy for cancer. *Bull Math Biol* **72**, 469–489.

65 Bajzer Z, Carr T, Josic K, Russell SJ & Dingli D (2008) Modeling of cancer virotherapy with recombinant measles viruses. *J Theor Biol* **252**, 109–122.
66 Reis CL, Pacheco JM, Ennis MK & Dingli D (2010) In silico evolutionary dynamics of tumour virotherapy. *Integr Biol (Camb)* **2**, 41–45.
67 Peng KW, Hadac EM, Anderson BD, Myers R, Harvey M, Greiner SM, Soeffker D, Federspiel MJ & Russell SJ (2006) Pharmacokinetics of oncolytic measles virotherapy: eventual equilibrium between virus and tumor in an ovarian cancer xenograft model. *Cancer Gene Ther* **13**, 732–738.
68 Wodarz D, Hofacre A, Lau JW, Sun Z, Fan H & Komarova NL (2012) Complex spatial dynamics of oncolytic viruses in vitro: mathematical and experimental approaches. *PLoS Comput Biol* **8**, e1002547.
69 Rodriguez-Brenes IA, Hofacre A, Fan H & Wodarz D (2017) Complex dynamics of virus spread from low infection multiplicities: implications for the spread of oncolytic viruses. *PLoS Comput Biol* **13**, e1005241.
70 Paiva LR, Binny C, Ferreira SC Jr & Martins ML (2009) A multiscale mathematical model for oncolytic virotherapy. *Cancer Res* **69**, 1205–1211.
71 Berg D, Offord C, Kemler I, Ennis M, Chang L, Paulik G, Bajzer Z, Neuhauser C & Dingli D (2019) In vitro and in silico multidimensional modeling of oncolytic tumor virotherapy dynamics. *PLoS Comput Biol* **15**, e1006773.
72 Miyagawa M, Anton M, Wagner B, Haubner R, Souvatzoglou M, Gansbacher B, Schwaiger M & Bengel FM (2005) Non-invasive imaging of cardiac transgene expression with PET: comparison of the human sodium/iodide symporter gene and HSV1-tk as the reporter gene. *Eur J Nucl Med Mol Imaging* **32**, 1108–1114.
73 Herschman HR (2002) Non-invasive imaging of reporter genes. *J Cell Biochem Suppl* **39**, 36–44.
74 Slooter GD, Mearadji A, Breeman WA, Marquet RL, de Jong M, Krenning EP & van Eijck CH (2001) Somatostatin receptor imaging, therapy and new strategies in patients with neuroendocrine tumours. *Br J Surg* **88**, 31–40.
75 Moroz MA, Serganova I, Zanzonico P, Ageyeva L, Beresten T, Dyomina E, Burnazi E, Finn RD, Doubrovin M & Blasberg RG (2007) Imaging hNET reporter gene expression with 124I-MIBG. *J Nucl Med* **48**, 827–836.
76 Ong HT, Hasegawa K, Dietz AB, Russell SJ & Peng KW (2007) Evaluation of T cells as carriers for systemic measles virotherapy in the presence of antiviral antibodies. *Gene Ther* **14**, 324–333.
77 Jung MY, Offord CP, Ennis MK, Kemler I, Neuhauser C & Dingli D (2018) In vivo estimation of oncolytic virus populations within tumors. *Cancer Res* **78**, 5992–6000.
78 Carlson SK, Classic KL, Hadac EM, Dingli D, Bender CE, Kemp BJ & Russell SJ (2009) Quantitative molecular imaging of viral therapy for pancreatic cancer using an engineered measles virus expressing the sodium-iodide symporter reporter gene. *AJR Am J Roentgenol* **192**, 279–287.
79 Penheiter AR, Griesmann GE, Federspiel MJ, Dingli D, Russell SJ & Carlson SK (2012) Pinhole micro-SPECT/CT for noninvasive monitoring and quantitation of oncolytic virus dispersion and percent infection in solid tumors. *Gene Ther* **19**, 279–287.
80 Miller A, Suksanpaisan L, Naik S, Nace R, Federspiel M, Peng KW & Russell SJ (2014) Reporter gene imaging identifies intratumoral infection voids as a critical barrier to systemic oncolytic virus efficacy. *Mol Ther Oncolytics* **1**, 14005.
81 Blommestein HM, Verelst SG, de Groot S, Huijgens PC, Sonneveld P & Uyl-de Groot CA (2015) A cost-effectiveness analysis of real-world treatment for elderly patients with multiple myeloma using a full disease model. *Eur J Haematol*.
82 Groot-Wassink T, Barthel H, Lemoine NR & Vassaux G (2003) Sodium iodide symporter: a new strategy to target cancer? *Lancet* **361**, 1905–1906.
83 Kemler I, Ennis MK, Neuhauser C & Dingli D. (2018) In vivo imaging of oncolytic measles virus propagation with single cell resolution, *Mol Ther - Oncol* **12**, 68–78.
84 Spitzweg C, Dietz AB, O'Connor MK, Bergert ER, Tindall DJ, Young CY & Morris JC (2001) In vivo sodium iodide symporter gene therapy of prostate cancer. *Gene Ther* **8**, 1524–1531.
85 Goel A, Carlson SK, Classic KL, Greiner S, Naik S, Power AT, Bell JC & Russell SJ (2007) Radioiodide imaging and radiovirotherapy of multiple myeloma using VSV(Delta51)-NIS, an attenuated vesicular stomatitis virus encoding the sodium iodide symporter gene. *Blood* **110**, 2342–2350.
86 Mansfield DC, Kyula JN, Rosenfelder N, Chao-Chu J, Kramer-Marek G, Khan AA, Roulstone V, McLaughlin M, Melcher AA, Vile RG *et al*. (2016) Oncolytic vaccinia virus as a vector for therapeutic sodium iodide symporter gene therapy in prostate cancer. *Gene Ther* **23**, 357–368.
87 Ennis MK, Hu C, Naik SK, Hallak LK, Peng KW, Russell SJ & Dingli D (2010) Mutations in the stalk region of the measles virus hemagglutinin inhibit syncytium formation but not virus entry. *J Virol* **84**, 10913–10917.
88 Corey EA & Iorio RM (2007) Mutations in the stalk of the measles virus hemagglutinin protein decrease fusion but do not interfere with virus-specific interaction with the homologous fusion protein. *J Virol* **81**, 9900–9910.

89 Groot-Wassink T, Aboagye EO, Wang Y, Lemoine NR, Reader AJ & Vassaux G (2004) Quantitative imaging of Na/I symporter transgene expression using positron emission tomography in the living animal. *Mol Ther* **9**, 436–442.

90 Dingli D, Bergert ER, Bajzer Z, O'Connor M & K., Russell, S. J. & Morris, J. C.(2004) Dynamic iodide trapping by tumor cells expressing the thyroidal sodium iodide symporter. *Biochem Biophys Res Commun* **325**, 157–166.

91 Kemler I, Neuhauser C & Dingli D (2018) Oncolytic virotherapy - in vivo veritas. *Oncotarget* **9**, 36254–36255.

92 Laschke MW, Vollmar B & Menger MD (2011) The dorsal skinfold chamber: window into the dynamic interaction of biomaterials with their surrounding host tissue. *Eur Cell Mater* **22**, 147–167.

93 Kemler I, Ennis MK, Neuhauser C & Dingli D (2019) In vivo imaging of oncolytic measles virus propagation with single cell resolution. *Molecular Therapy - Oncolytics* **12**, 68–79.

94 Bailey K, Kirk A, Naik S, Nace R, Steele MB, Suksanpaisan L, Li X, Federspiel MJ, Peng KW, Kirk D *et al.* (2013) Mathematical model for radial expansion and conflation of intratumoral infectious centers predicts curative oncolytic virotherapy parameters. *PLoS One* **8**, e73759.

95 Kumar A, Kim JH, Ranjan P, Metcalfe MG, Cao W, Mishina M, Gangappa S, Guo Z, Boyden ES, Zaki S *et al.* (2017) Influenza virus exploits tunneling nanotubes for cell-to-cell spread. *Sci Rep* **7**, 40360.

96 Roberts KL, Manicassamy B & Lamb RA (2015) Influenza A virus uses intercellular connections to spread to neighboring cells. *J Virol* **89**, 1537–1549.

97 Cifuentes-Munoz N, Dutch RE & Cattaneo R (2018) Direct cell-to-cell transmission of respiratory viruses: The fast lanes. *PLoS Pathog* **14**, e1007015.

98 Liu C, Russell SJ & Peng KW (2010) Systemic therapy of disseminated myeloma in passively immunized mice using measles virus-infected cell carriers. *Mol Ther* **18**, 1155–1164.

99 Cole C, Qiao J, Kottke T, Diaz RM, Ahmed A, Sanchez-Perez L, Brunn G, Thompson J, Chester J & Vile RG (2005) Tumor-targeted, systemic delivery of therapeutic viral vectors using hitchhiking on antigen-specific T cells. *Nat Med* **11**, 1073–1081.

100 Ilett EJ, Prestwich RJ, Kottke T, Errington F, Thompson JM, Harrington KJ, Pandha HS, Coffey M, Selby PJ, Vile RG *et al.* (2009) Dendritic cells and T cells deliver oncolytic reovirus for tumour killing despite pre-existing anti-viral immunity. *Gene Ther* **16**, 689–699.

101 Shen W, Patnaik MM, Ruiz A, Russell SJ & Peng KW (2016) Immunovirotherapy with vesicular stomatitis virus and PD-L1 blockade enhances therapeutic outcome in murine acute myeloid leukemia. *Blood* **127**, 1449–1458.

102 Peng KW, Myers R, Greenslade A, Mader E, Greiner S, Federspiel MJ, Dispenzieri A & Russell SJ (2013) Using clinically approved cyclophosphamide regimens to control the humoral immune response to oncolytic viruses. *Gene Ther* **20**, 255–261.

103 Escobar-Zarate D, Liu YP, Suksanpaisan L, Russell SJ & Peng KW (2013) Overcoming cancer cell resistance to VSV oncolysis with JAK1/2 inhibitors. *Cancer Gene Ther* **20**, 582–589.

104 Jung BK, Ko HY, Kang H, Hong J, Ahn HM, Na Y, Kim H, Kim JS & Yun CO (2020) Relaxin-expressing oncolytic adenovirus induces remodeling of physical and immunological aspects of cold tumor to potentiate PD-1 blockade. *J Immunother Cancer* **8**, 763.

105 Everts A, Bergeman M, McFadden G & Kemp V (2020) Simultaneous tumor and stroma targeting by oncolytic viruses. *Biomedicines* **8**, 474.